Vietnam Journal of Catalysis and Adsorption
Tạp chí xúc tác và hấp phụ Việt Nam

https://jca.edu.vn

Synthesis of AgNPs@aerogel cellulose material from sugarcane bagasse for antibiotic removal in water: Kinetic evaluation and process optimization

Hoa Nguyen Thi[1,*], Ngoc Hoang Minh[2,†], Nguyen Mai Trung[2,†], Duong Nguyen Thuy[2,†], Duc Tran Minh[2,†], Duy Nguyen Luong Thai[2,†]

[1] *Global Science Journey Joint Stock Company (GSJ), 33/10 Nguyen Thi Dinh Street, Yen Hoa Ward, Hanoi, Vietnam*
[2] *Hanoi – Amsterdam High School for the Gifted, 1 Hoang Minh Giam Street, Yen Hoa Ward, Hanoi, Vietnam*
** Email: hoa41154@gmail.com*
† All authors contributed equally to this work

ARTICLE INFO

Received: 28/11/2025
Accepted: 30/12/2025
Published: 30/12/2025

Keywords:
AgNPs@cellulose aerogel;
Green synthesis;
Photocatalytic degradation;
Tetracycline removal;
Sugarcane bagasse

ABSTRACT

Antibiotic contamination has emerged as a critical global concern due to the excessive use of pharmaceuticals in medicine and livestock production, leading to their persistent accumulation in aquatic environments. Conventional treatment methods often show limited efficiency, high cost, or environmental drawbacks, highlighting the urgent need for sustainable alternatives. In this study, a green, porous AgNPs@cellulose aerogel composite was successfully synthesized using purified cellulose from sugarcane bagasse and lotus leaf extract as a natural reducing agent for silver nanoparticle formation. The structural and physicochemical properties of the materials were thoroughly characterized by XRD, SEM, BET, and UV–Vis analyses. XRD results confirmed the incorporation of crystalline AgNPs within the cellulose matrix, while SEM images revealed a well-preserved porous network with uniformly dispersed nanoparticles. BET analysis showed an increase in specific surface area from 70 to 87.2 m^2/g after silver loading, indicating enhanced porosity. The optical band gap decreased with increasing AgNP content, demonstrating improved visible-light absorption capacity. Photocatalytic experiments showed that the AgNPs@cellulose aerogel exhibited significantly enhanced tetracycline (TC) degradation under visible light, achieving up to 95% removal under optimal conditions. Kinetic studies revealed that the TC degradation followed pseudo–first-order kinetics with high correlation coefficients (R^2 > 0.96). The photocatalyst also demonstrated excellent reusability, maintaining over 85% efficiency after four cycles. These findings highlight the potential of AgNPs@cellulose aerogel as an effective, eco-friendly, and sustainable photocatalyst for antibiotic removal from wastewater.

Introduction

Antibiotics are widely used in the treatment of bacterial infections, as well as in promoting livestock growth and feed efficiency. According to R. Daghrir and P. Drogui [1], the global annual consumption of these pharmaceuticals has reached approximately 100,000 – 200,000 tons. However, the excessive and uncontrolled use of antibiotics has resulted in their accumulation in various aquatic environments, including surface water, groundwater, drinking water, and wastewater [2][3]. This persistent presence poses serious risks to both human

©2025 by the authors. Licensee Vietnam Journal of Catalysis and Adsorption. This article is an open access article distributed under the terms and conditions of the Creative Commons Attribution (CC BY) license (https://creativecommons.org/licenses/by/4.0/).

https://doi.org/10.62239/jca.2025.071

health and ecological systems. In particular, antibiotics released into soil and aquatic environments can alter the physiological balance of microorganisms such as microalgae, disrupt aquatic ecosystems, and accelerate the emergence of antibiotic-resistant pathogens - one of the leading causes of mortality worldwide.

Conventional methods for antibiotic removal, such as physical, chemical, and biological processes, often exhibit critical drawbacks. Physical approaches (e.g., membrane filtration) cannot completely eliminate antibiotic residues and are prone to membrane fouling due to the presence of salts and organic matter [4]. Chemical oxidation methods, while effective to some extent, often require hazardous reagents, are cost-ineffective, and involve high energy consumption. Biological methods, although environmentally friendly, demand highly skilled operations and complex instrumentation (such as PCR and electrophoresis), resulting in time-consuming procedures that are typically employed only as supporting techniques [5]. Therefore, it is imperative to develop more efficient, economical, and sustainable technologies for antibiotic removal from water systems [6].

Among advanced treatment strategies, photocatalysis has emerged as a promising green technology for the degradation of persistent organic pollutants (POPs), owing to its high efficiency, low secondary pollution, and potential for solar energy utilization [7,8]. In this regard, silver nanoparticles (AgNPs) have drawn significant attention because of their remarkable photocatalytic activity, stability, and strong oxidative properties toward various organic contaminants [9]. Nevertheless, their application can be limited by aggregation tendencies and slow adsorption kinetics in aqueous media [10].

To overcome these challenges, aerogels - lightweight, highly porous materials with large specific surface areas - have been explored as excellent supports for dispersing and stabilizing photocatalysts [11,12]. Traditional inorganic aerogels (e.g., silica-based) often suffer from toxicity and non-biodegradability, restricting their environmental applications [13]. In contrast, cellulose-based aerogels offer a renewable, biocompatible, and biodegradable alternative, combining the advantages of aerogels' structural features with the green characteristics of natural polymers [14]. Thus, the integration of AgNPs into cellulose aerogel matrices is expected to create a synergistic photocatalyst with enhanced adsorption, stability, and photocatalytic degradation efficiency for antibiotic removal from aqueous environments.

Experimental

Materials and chemicals

Cellulose was extracted from sugarcane bagasse collected locally in Vietnam through an alkaline–bleaching treatment process. Silver nitrate ($AgNO_3$, ≥99.8%) was purchased from Sigma-Aldrich and used as the silver precursor for nanoparticle synthesis. Fresh lotus leaves (Nelumbo nucifera) were obtained from a local market and employed as a natural reducing and stabilizing agent for the preparation of Ag nanoparticles. Tetracycline hydrochloride (TC, ≥98%) was supplied by Merck and used as the target contaminant in photocatalytic experiments. Ethanol (99.5%), sodium hydroxide (NaOH), hydrochloric acid (HCl), and other analytical-grade chemicals were obtained from Xilong Chemical and used without further purification.

Purification of Cellulose

The purification of cellulose from sugarcane bagasse was carried out in two main stages. Initially, 10 g of raw bagasse pulp was treated with 100 mL of 1 M NaOH solution under reflux conditions for 1 hour to remove hemicellulose, lignin, and other non-cellulosic impurities. The resulting cellulose residue was repeatedly washed with distilled water until the filtrate reached a neutral pH (pH=7), ensuring complete removal of excess alkali.

In the subsequent bleaching step, the purified cellulose was refluxed for 1 hour in a mixed solution containing 1% NaClO and 1% NaOH. After bleaching, the cellulose fibers were separated by vacuum filtration using filter paper and thoroughly rinsed with water before drying for further use.

Preparation of Cellulose Aerogel

The refined cellulose was finely ground and blended with a polyvinyl alcohol (PVA) solution in a 1:1 weight ratio using 50 mL of distilled water as the solvent. The homogeneous suspension was then frozen at -20 °C for 24 hours to induce gel formation. Afterward, the frozen hydrogel was freeze-dried at -50 °C to -70 °C to sublimate the ice crystals, yielding a lightweight, porous cellulose aerogel.

Preparation of AgNPs@Cellulose Aerogel

The experiment examined whether the lotus-leaf extract's bioactive compounds hold the role of acting as a reducing agent for silver ions to form metallic silver. The solution of $AgNO_3$ was introduced first, followed by Polyvinyl Alcohol (PVA) and lotus leaf extract. By then,

https://doi.org/10.62239/jca.2025.071

the clear solution turned from yellow to brown - a visual cue that silver nanoparticles had formed. On the other hand, PVA chains stabilize and protect nascent AgNPs from agglomeration.

First, the lotus leaf extract is created from the reflux extraction method. Lotus leaf is grinded to a coarse powder and mixed with water in the ratio of 1:10. The solution is heated to gentle boiling, and reflux is maintained for 1 hour while stirring steadily. After boiling, the mixture is filtered to obliterate any residue; by then, only the lotus leaf extract is left. Finally, we store the aqueous extract at 4 °C in the refrigerator, protected from light and moisture.

To be exact, the process started by dissolving 0.17 g of Silver Nitrate ($AgNO_3$) in 100 mL of water and stirring the solution for 30 minutes. We then added 0.17 g of Polyvinyl Alcohol (PVA), followed by 14 mL of lotus-leaf extract. The mixture was left to react for a further two hours, setting the stage for nanoparticle formation. The entire condition is in the dark, with no direct contact with UV sunlight.

The attained AgNPs is then added to aerogel cellulose and mixed thoroughly for 30 minutes. The homogeneous suspension was then frozen at -20 °C for 24 hours to induce gel formation. Afterward, the frozen hydrogel was freeze-dried at -50 °C to -70 °C to sublimate the ice crystals.

Characterization

The structural and physicochemical properties of the samples were analyzed using several techniques. X-ray diffraction (XRD) (Bruker D8 Advance, Cu Kα radiation) was used to identify the crystalline structure of cellulose aerogel and the formation of Ag nanoparticles. Scanning electron microscopy (SEM) (JEOL JSM-7600F) was employed to observe the morphology and distribution of AgNPs within the aerogel network. Nitrogen adsorption–desorption (BET) measurements (Micromeritics ASAP 2020) determined the specific surface area and pore characteristics after degassing at 120°C. UV–Vis diffuse reflectance spectroscopy (UV–Vis DRS) (Shimadzu UV-2600) was used to evaluate optical absorption and estimate the band gap using Tauc plots. FTIR spectroscopy (Nicolet iS10) was conducted to identify functional groups and confirm chemical interactions among cellulose, lotus extract, and AgNPs.

Investigation of photocatalyst activity

A tetracycline (TC) stock solution with a concentration of 50 ppm was first prepared by dissolving 5 mg of tetracycline powder in 100 mL of deionized water. Subsequently, 35 mL of this TC solution was transferred into a reaction vessel and mixed with 50 mg of the AgNPs@cellulose aerogel photocatalyst to form the photocatalyst-TC suspension. The suspension was kept in the dark for 30 min to establish the adsorption–desorption equilibrium. After equilibration, the mixture was irradiated under a light source for 4 h to initiate the photocatalytic degradation process. At 1 h intervals, approximately 3 mL of the reaction mixture was withdrawn, filtered, and analyzed using a UV-Vis spectrophotometer to monitor the remaining TC concentration.

The photocatalytic degradation efficiency was calculated according to the following equation:

$$H(\%) = \frac{C_0 - C_t}{C_0} \times 100 \qquad (1)$$

where: C_0 is the initial concentration of tetracycline, C_t is the tetracycline concentration at irradiation time t, and $H(\%)$ is the degradation efficiency at time t.

Results and discussion

The XRD patterns of the cellulose aerogel and AgNPs@cellulose aerogel are presented in Figure 1. The cellulose aerogel exhibits a broad diffraction peak centered at approximately 2θ = 22°, corresponding to the (200) crystallographic plane of cellulose I, along with a weak shoulder near 2θ = 16°, assigned to the (101) plane. These features are consistent with the typical diffraction behavior of regenerated cellulose I reported in previous studies [15,16], confirming that the cellulose framework is preserved after aerogel formation, albeit with reduced crystallinity due to structural disruption during regeneration.

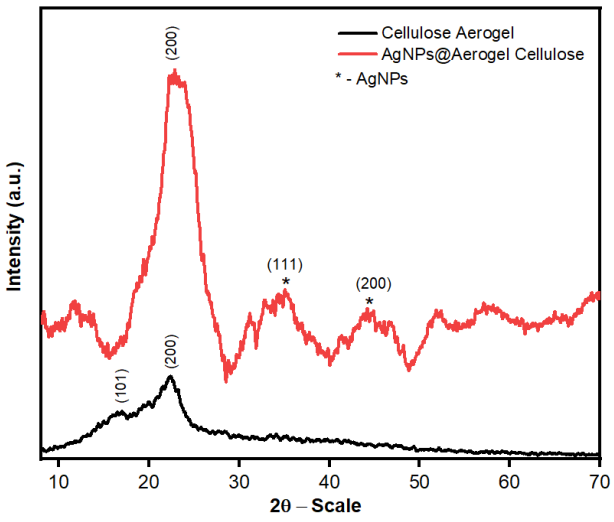

Fig. 1: X-ray diffraction of cellulose and AgNPs@cellulose aerogel

In contrast, the AgNPs@cellulose aerogel shows several additional diffraction peaks at 2θ = 38° and 44°, which correspond to the (111) and (200) planes of face-centered cubic (fcc) metallic silver, respectively. These peaks match well with standard Ag diffraction data (JCPDS No. 04-0783) and with previously reported AgNPs synthesized on biopolymer supports [17][18]. Their appearance unambiguously verifies the successful formation of AgNPs within the cellulose aerogel matrix. A noticeable increase in the intensity of the cellulose (200) peak is observed for the AgNPs-loaded sample. This enhancement may be attributed to the strong interaction between AgNPs and the hydroxyl-rich cellulose network, which induces local ordering and increases the electron density within the composite, similar to observations reported in AgNP–cellulosic hybrid systems [19]. The slight signal broadening and background noise in the 40–70° region further indicate the presence of small-sized, well-dispersed AgNPs. Overall, the XRD results confirm that the cellulose structure is maintained while AgNPs are successfully anchored within the aerogel network, forming a hybrid composite material exhibiting characteristic crystalline silver signatures.

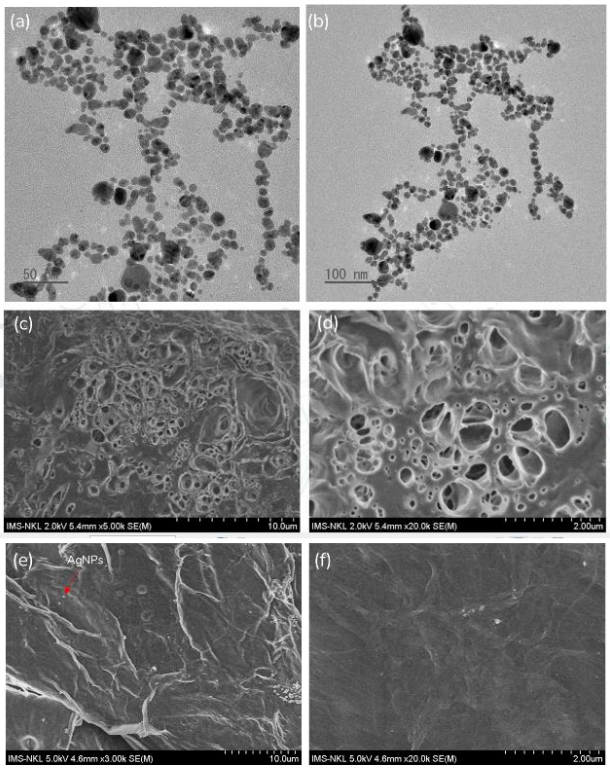

Fig. 2. (a,b) TEM images of AgNPs, SEM images of (c,d) cellulose aerogel and (e,f) AgNPs@cellulose aerogel

Transmission electron microscopy (TEM) was employed to further investigate the morphology, size distribution, and dispersion state of AgNPs (Figure 2 a,b). The TEM images reveal that the silver nanoparticles are predominantly spherical with relatively narrow size distribution, ranging from approximately 8 to 20 nm. The AgNPs are uniformly dispersed without noticeable agglomeration, indicating that the bioactive compounds present in the lotus leaf extract effectively act as both reducing and stabilizing agents during nanoparticle formation. The small particle size and homogeneous dispersion of AgNPs are highly favorable for photocatalytic applications, as they provide a large number of accessible active sites and promote strong localized surface plasmon resonance (LSPR) under visible-light irradiation. SEM images of the cellulose aerogel and AgNPs@cellulose aerogel are presented in Figure 2(c–f). In images (c) and (d), the cellulose aerogel exhibits a three-dimensional porous architecture with numerous voids of varying sizes uniformly distributed across the surface. This morphology is characteristic of aerogel materials, which possess high porosity, large specific surface area, and an interconnected cellulose network that facilitates diffusion and adsorption processes. After the incorporation of silver nanoparticles (AgNPs), images (e) and (f) of the AgNPs@cellulose aerogel show that the surface becomes smoother and denser, partly due to AgNPs occupying the micro- and mesopores of the cellulose framework. The bright spots, homogeneously dispersed on the surface, correspond to nanoscale AgNPs that are well-anchored within the polymeric network. The clear appearance of these particles confirms the effective reduction of Ag^{+} ions to metallic Ag^{0} and their uniform dispersion throughout the aerogel structure. The SEM results indicate that the AgNPs are not only successfully formed but also stably distributed, which contributes to the enhanced electrical conductivity, antibacterial performance, and photocatalytic activity of the composite material.

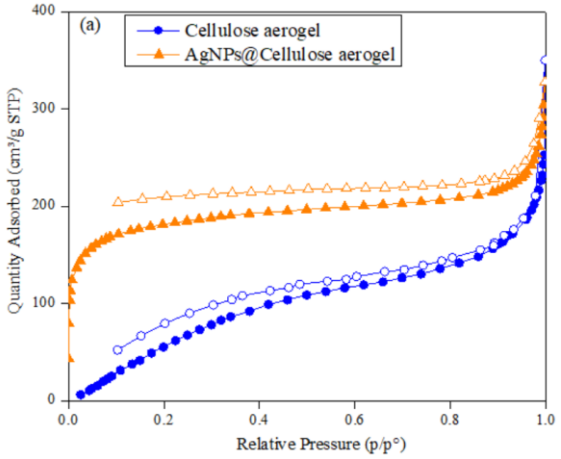

Fig. 3. BET nitrogen adsorption–desorption isotherms of cellulose aerogel and AgNPs@cellulose aerogel

The N_2 adsorption–desorption isotherms of the cellulose aerogel and AgNPs@cellulose aerogel are shown in Figure 3.3. Both samples exhibit adsorption curves characteristic of mesoporous materials (type IV according to the IUPAC classification), accompanied by an H3 hysteresis loop at high relative pressures (p/p° > 0.8), indicating the presence of slit-shaped pores formed between the cellulose layers. Compared with the cellulose aerogel, the AgNPs@cellulose aerogel displays a markedly higher adsorbed gas volume over the entire pressure range, reflecting the enhanced adsorption capacity of the material after AgNP loading.

BET analysis shows that the specific surface area of the cellulose aerogel increases from 70 m^2/g to 87.2 m^2/g after the incorporation of silver nanoparticles. This increase can be attributed to the formation of small AgNPs uniformly distributed throughout the cellulose network, which contributes to the expansion and stabilization of the pore structure. In addition, interactions between AgNPs and the hydroxyl groups of cellulose help prevent structural shrinkage during the drying process, thereby preserving the high porosity of the material. These results demonstrate that the integration of AgNPs not only imparts photocatalytic and antibacterial functionalities but also improves the morphological characteristics and specific surface area of the cellulose aerogel.

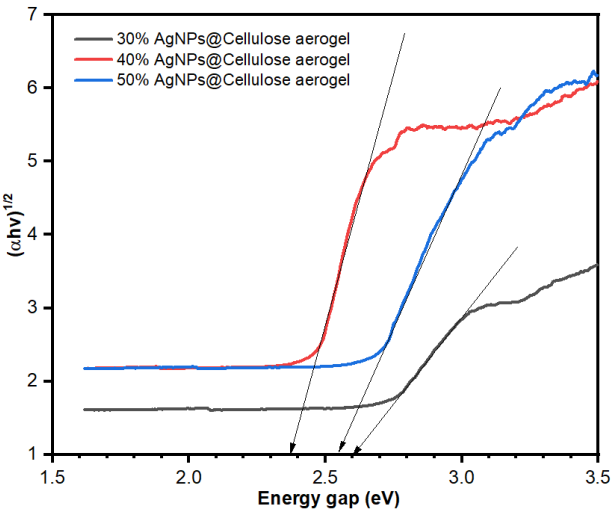

Fig. 4. Energy gap of 30-50% AgNPs@cellulose aerogel

The Tauc plots of $(\alpha h\nu)^{1/2}$ as a function of photon energy for the AgNPs@cellulose aerogel samples with AgNP loadings of 30%, 40%, and 50% reveal noticeable variations in their optical properties. With increasing AgNP content, the absorption edge generally shifts toward lower photon energies (red shift), indicating an overall reduction in the band gap energy (Eg). The sample containing 30% AgNPs exhibits the highest Eg of approximately 2.60 eV, while a pronounced red shift is observed for the 40% AgNP-loaded sample, resulting in a reduced Eg of about 2.38 eV.

Notably, although the 50% AgNP sample still shows a red-shifted absorption edge compared to the 30% sample, its Eg slightly increases to 2.55 eV relative to the 40% sample. This deviation from a strictly monotonic trend may be attributed to factors such as AgNP agglomeration at higher loadings, changes in nanoparticle-cellulose interactions, or increased light scattering, which can partially counteract the band gap narrowing effect. Therefore, the reduction in Eg with AgNP incorporation is mainly associated with the introduction of localized energy states and the localized surface plasmon resonance (LSPR) effect of AgNPs, enhancing visible-light absorption in the composite aerogels.

These findings demonstrate that the incorporation of AgNPs not only alters the pore structure of the cellulose aerogel but also enriches the electronic states within the band gap, making the material more easily photoexcited. This behavior is particularly beneficial for applications such as photocatalysis, light-activated antibacterial systems, and optical sensing, where strong visible-light absorption plays a crucial role. Thus, increasing the AgNP content significantly improves the optical properties of the AgNPs@cellulose aerogel composite and broadens its potential applications in photoactive material systems.

Evaluation of Photocatalytic Activity

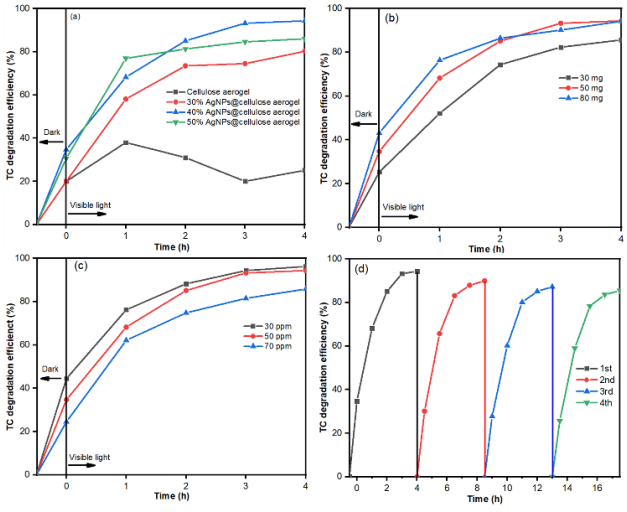

Fig. 5. The degradation of TC under visible light using AgNPs@Cellulose aerogel catalyst under the conditions of (a) contents of the active phase, (b) catalyst dosage, (c) TC concentration, (d) photocatalyst regenerability

https://doi.org/10.62239/jca.2025.071

Figure 5(a) illustrates the tetracycline (TC) degradation efficiency over time for the cellulose aerogel and the AgNPs@cellulose aerogel composite samples with different silver loadings (30%, 40%, and 50%). The results show that the TC removal efficiency of all samples increases with reaction time, with AgNP-containing materials exhibiting significantly higher degradation performance compared to the pristine cellulose aerogel. After 1 hour, the 50%AgNPs@cellulose aerogel sample achieved a removal efficiency of approximately 78%, which is notably higher than that of the 40%AgNPs@cellulose aerogel (70%), 30%AgNPs@cellulose aerogel (55%), and the cellulose aerogel (40%). When the reaction time reached 4 hours, the removal efficiencies tended to approach equilibrium: the 50%AgNPs@cellulose aerogel (90%) and 40%AgNPs@cellulose aerogel (88%) exhibited nearly comparable performance, whereas the 30% sample reached about 80% and the cellulose aerogel only attained 65%. The enhancement in efficiency with increasing AgNPs content indicates the photocatalytic role of silver nanoparticles, which promote stronger light absorption and the generation of more reactive species (•OH, $•O_2^-$), thereby accelerating TC degradation. However, when the Ag content exceeded 40%, the improvement was not substantial, likely due to AgNP aggregation, which reduces the active surface area and hinders charge transfer. Therefore, the 40%AgNPs@cellulose aerogel sample can be considered the optimal material, offering high degradation efficiency while maintaining a balance between photocatalytic activity and structural stability.

A clear correlation can be established between AgNP loading, band-gap energy variation, and tetracycline degradation efficiency. As the AgNP content increased from 30% to 40%, the band gap decreased significantly from 2.60 to 2.38 eV, corresponding to enhanced visible-light absorption and higher photocatalytic activity. This reduction in Eg directly translated into increased TC degradation efficiency, rising from approximately 80% to nearly 90% after 4 hours. However, further increasing AgNP content to 50% resulted in only a marginal change in band gap and photocatalytic performance, indicating that excessive AgNPs do not contribute proportionally to activity enhancement. This behavior suggests an optimal balance between plasmonic enhancement, charge transfer efficiency, and active surface availability at 40% AgNP loading.

Figure 5(b) illustrates the effect of the catalyst mass of AgNPs@cellulose aerogel on the photocatalytic degradation efficiency of tetracycline (TC) as a function of reaction time. The results show that the TC removal efficiency gradually increases as the catalyst mass increases from 30 mg to 80 mg. After 1 hour of reaction, the degradation efficiencies were approximately 52% for 30 mg, 70% for 50 mg, and 78% for 80 mg. When the reaction time was extended to 4 hours, these values increased to 86%, 93%, and 95%, respectively. The enhanced performance with higher catalyst dosage can be attributed to the increased number of active sites and greater contact area between the catalyst and TC molecules, which promotes adsorption and the formation of reactive oxygen species (•OH, $•O_2^-$) under light irradiation. However, when the catalyst mass increases from 50 mg to 80 mg, the improvement becomes marginal due to the limited availability of incident light. Therefore, 50 mg can be considered the optimal catalyst dosage, offering high degradation efficiency (above 90%) while maintaining economic feasibility and reasonable energy utilization.

Figure 5(c) presents the effect of tetracycline (TC) concentration on the photocatalytic degradation efficiency using the AgNPs@cellulose aerogel material. The results show that as the TC concentration increases from 30 ppm to 70 ppm, the degradation efficiency gradually decreases under the same irradiation and reaction conditions. After 4 hours, the degradation efficiencies were approximately 96% (30 ppm), 92% (50 ppm), and only 85% (70 ppm). The reduction in efficiency at higher TC concentrations can be explained as follows: At low concentrations (30 ppm), the number of TC molecules is moderate, allowing light to effectively reach the catalyst surface, thereby maximizing the activation of active sites and the generation of reactive oxygen species (•OH, $•O_2^-$) for rapid TC degradation. When the TC concentration increases, more organic molecules adsorb onto the catalyst surface, reducing the number of available active sites and limiting photon penetration into the solution. Therefore, the results indicate that an initial TC concentration of 30–50 ppm is optimal for treatment using the AgNPs@cellulose aerogel material, ensuring high degradation efficiency while maintaining a balance between adsorption capacity and photocatalytic activity.

The recyclability of the AgNPs@cellulose aerogel photocatalyst was evaluated over four consecutive degradation cycles of tetracycline (TC), as illustrated in Figure 5(d). The results demonstrate that the catalyst maintains high photocatalytic activity throughout repeated use, indicating excellent structural stability and regenerability. In the first cycle, the TC degradation

https://doi.org/10.62239/jca.2025.071

efficiency reached nearly 95% within 4 hours. Although a slight decrease in performance was observed in subsequent cycles, the catalyst still achieved approximately 92% in the second cycle, 89% in the third cycle, and 86% in the fourth cycle, even though the reaction time was extended accordingly to reach comparable degradation levels. The minor decline in activity can be attributed to partial blockage of active sites by residual organic intermediates adsorbed on the catalyst surface or slight surface fouling during repeated reactions. Nevertheless, the overall high retention of photocatalytic efficiency (over 85% after four cycles) confirms that AgNPs are firmly anchored within the aerogel matrix, preventing leaching and maintaining their plasmonic activity. These findings highlight the good recyclability and long-term operational stability of the AgNPs@cellulose aerogel, making it a promising material for practical wastewater treatment applications.

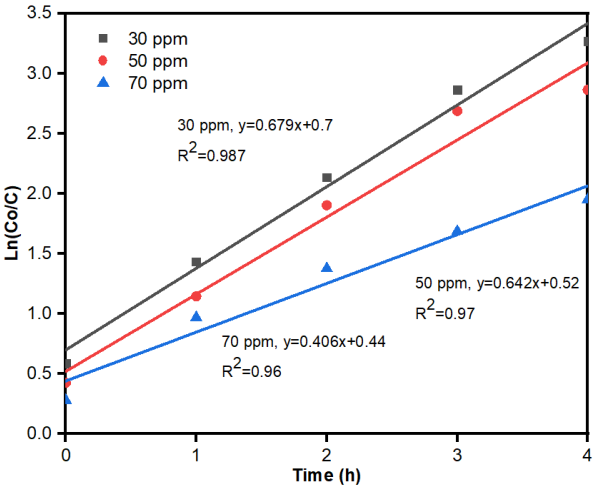

Fig. 6. First-order kinetics model for AgNP@Cellulose aerogel sample

The photocatalytic degradation kinetics of tetracycline (TC) over the AgNPs@cellulose aerogel were analyzed using the pseudo–first-order kinetic model, expressed as $\ln(C_0/C) = kt$. As shown in Figure 3.8, the linear fitting curves for TC concentrations of 30, 50, and 70 ppm exhibit strong linearity, with correlation coefficients (R^2) of 0.987, 0.970, and 0.960, respectively. These high R^2 values indicate that the photocatalytic degradation process follows pseudo–first-order kinetics, suggesting that the reaction rate is predominantly governed by the concentration of adsorbed TC molecules on the catalyst surface. The calculated rate constants (k) decrease with increasing TC concentration: k = 0.679 h^{-1} (30 ppm), 0.642 h^{-1} (50 ppm), and 0.406 h^{-1} (70 ppm). This trend reflects the inhibitory effect of higher pollutant concentrations, where excessive TC molecules occupy more active sites, limiting photon absorption and restricting the generation of reactive oxygen species (•OH, $•O_2^-$). Consequently, lower concentrations allow faster reaction rates due to more efficient interaction between light, the catalyst, and TC molecules. Therefore, the kinetic analysis confirms that the AgNPs@cellulose aerogel exhibits efficient photocatalytic performance, and the pseudo–first-order model provides a reliable description of the TC degradation mechanism under the studied conditions.

The enhanced photocatalytic performance of the AgNPs@cellulose aerogel can be attributed to the synergistic contribution of three key factors: (i) the localized surface plasmon resonance (LSPR) effect of AgNPs, (ii) improved charge separation and interfacial electron transfer, and (iii) the adsorption capability of the cellulose aerogel matrix [20]. Under visible-light irradiation, AgNPs exhibit strong LSPR excitation, generating energetic "hot electrons" that can be readily transferred to the surrounding cellulose matrix or adsorbed oxygen molecules [21]. This plasmon-induced electron injection effectively increases the population of reactive electrons, which subsequently react with dissolved O_2 to form superoxide radicals ($•O_2^-$), while the remaining holes participate in hydroxyl radical (•OH) generation [22]. These reactive oxygen species play a dominant role in the oxidative degradation of tetracycline molecules [1]. In addition, the intimate interfacial contact between AgNPs and the cellulose aerogel facilitates efficient charge separation by acting as an electron sink, thereby suppressing electron–hole recombination [23]. The reduction in band-gap energy observed with increasing AgNP content further supports the improved photoexcitation efficiency and charge mobility within the composite system [24]. Meanwhile, the highly porous cellulose aerogel provides abundant adsorption sites for tetracycline through hydrogen bonding and π–π interactions, ensuring close proximity between pollutant molecules and reactive species [14]. This adsorption–photocatalysis coupling significantly enhances degradation kinetics, particularly at moderate AgNP loadings. However, excessive AgNP content leads to partial nanoparticle aggregation, which can shield active sites and hinder light penetration, explaining why the photocatalytic efficiency does not increase proportionally beyond 40% AgNP loading.

Conclusion

In this study, a green and sustainable AgNPs@cellulose aerogel photocatalyst was successfully synthesized using cellulose extracted from sugarcane bagasse and lotus leaf extract as a natural reducing agent. Structural

and morphological analyses confirmed the uniform formation and stable incorporation of nanosized AgNPs within the highly porous cellulose aerogel network, resulting in an increased specific surface area and enhanced visible-light absorption due to band-gap narrowing and localized surface plasmon resonance effects. The synergistic interaction between AgNPs and the cellulose aerogel not only improved charge separation and inhibited electron–hole recombination but also promoted effective adsorption of tetracycline molecules, thereby facilitating photocatalytic degradation. Photocatalytic experiments demonstrated that the composite exhibited excellent tetracycline removal efficiency under visible-light irradiation, following pseudo–first-order kinetics, with the 40% AgNP-loaded sample achieving optimal performance. Furthermore, the photocatalyst maintained more than 85% of its initial activity after four consecutive cycles, confirming its structural stability and resistance to silver leaching. Overall, the AgNPs@cellulose aerogel represents a promising eco-friendly and cost-effective photocatalytic material for antibiotic removal in wastewater treatment, offering a viable approach toward sustainable environmental remediation.

References

1. R. Daghrir, P. Drogui, Environ. Chem. Lett., 11(3) (2013) 209-227. https://doi.org/10.1007/s10311-013-0402-2
2. K. Kümmerer, Chemosphere, 75(4) (2009) 417-434. https://doi.org/10.1016/j.chemosphere.2009.01.077
3. J.L. Martinez, Environ. Pollut., 157(11) (2009) 2893-2902. https://doi.org/10.1016/j.envpol.2009.05.026
4. L.D. Nghiem, A. Manis, K. Soldenhoff, A.I. Schäfer, J. Memb. Sci., 242(1-2) (2004) 37-45. https://doi.org/10.1016/j.memsci.2004.05.008
5. T.A. Ternes, M. Meisenheimer, D. McDowell, F. Sacher, H.J. Brauch, B. Haist-Gulde, G. Preuss, U. Wilme, N. Zulei-Seibert, Environ. Sci. Technol., 36(17) (2002) 3855-3863. https://doi.org/10.1021/es020272o
6. J.L. Sanz, T. Köchling, Process Biochem., 42(2) (2007) 119-133. https://doi.org/10.1016/j.procbio.2006.07.031
7. N.T. Hoa, V.V. Tai, P.X. Nui, Vietnam J. Catal. Adsorpt., 10(4) (2021) 125-136. https://doi.org/10.51316/jca.2021.078
8. M.N. Chong, B. Jin, C.W.K. Chow, C. Saint, Water Res., 44(10) (2010) 2997-3027. https://doi.org/10.1016/j.watres.2010.02.039
9. X. Liang, Y. Li, X. Li, L. Jing, Z. Deng, Q. Yue, C. Li, Z. Dai, Adv. Funct. Mater., 25(10) (2015) 1451-1462. https://doi.org/10.1002/adfm.201404099
10. V.K. Sharma, R.A. Yngard, Y. Lin, Adv. Colloid Interface Sci., 145(1-2) (2009) 83-96. https://doi.org/10.1016/j.cis.2008.09.003
11. A.C. Pierre, G.M. Pajonk, Chem. Rev., 102(11) (2002) 4243-4266. https://doi.org/10.1021/cr010123j
12. N.T. Hoa, N.T. Tien, V.V. Tai, P.X. Nui, Vietnam J. Catal. Adsorpt., 10(4) (2021) 6-17. https://doi.org/10.51316/jca.2021.066
13. S. Zhao, W.J. Malfait, N. Guerrero-Alburquerque, M.M. Koebel, G. Nyström, Angew. Chem. Int. Ed., 57(26) (2018) 7580-7608. https://doi.org/10.1002/anie.201710014
14. L.Y. Long, Y.X. Weng, Y.Z. Wang, Polymers, 10(6) (2018) 623. https://doi.org/10.3390/polym10060623
15. H. Kargarzadeh, I. Ahmad, S. Thomas, A. Dufresne, Handbook of Nanocellulose and Cellulose Nanocomposites, John Wiley & Sons, 2017.
16. W. Chen, H. Yu, Y. Liu, P. Chen, M. Zhang, Y. Hai, Carbohydr. Polym., 83(4) (2011) 1804-1811. https://doi.org/10.1016/j.carbpol.2010.10.039
17. I. Sondi, B. Salopek-Sondi, J. Colloid Interface Sci., 275(1) (2004) 177-182. https://doi.org/10.1016/j.jcis.2004.02.012
18. S. Pal, Y.K. Tak, J.M. Song, Appl. Environ. Microbiol., 73(6) (2007) 1712-1720. https://doi.org/10.1128/AEM.00176-06
19. P. Lu, Y.-L. Hsieh, Carbohydr. Polym., 82(2) (2010) 329-336. https://doi.org/10.1016/j.carbpol.2010.05.020
20. S. Linic, P. Christopher, D.B. Ingram, Nat. Mater., 10(12) (2011) 911-921. https://doi.org/10.1038/nmat3151
21. H. Zhang, G. Chen, Environ. Sci. Technol., 43(8) (2009) 2905-2910. https://doi.org/10.1021/es803450f
22. J. Low, B. Cheng, J. Yu, Appl. Surf. Sci., 392 (2017) 658-686. https://doi.org/10.1016/j.apsusc.2016.09.093
23. X. Chen, S. Shen, L. Guo, S.S. Mao, Chem. Rev., 110(11) (2010) 6503-6570. https://doi.org/10.1021/cr1001645
24. J. Yu, J. Low, W. Xiao, P. Zhou, M. Jaroniec, J. Am. Chem. Soc., 136(25) (2014) 8839-8842. https://doi.org/10.1021/ja5042852